

Monitoring and assessment of soil erosion at micro-scale and macro-scale in forests affected by fire damage in northern Iran

Ali Akbarzadeh · Shoja Ghorbani-Dashtaki ·
Mehdi Naderi-Khorasgani · Ruth Kerry ·
Ruhollah Taghizadeh-Mehrjardi

Received: 28 May 2016 / Accepted: 18 November 2016 / Published online: 29 November 2016
© Springer International Publishing Switzerland 2016

Abstract Understanding the occurrence of erosion processes at large scales is very difficult without studying them at small scales. In this study, soil erosion parameters were investigated at micro-scale and macro-scale in forests in northern Iran. Surface erosion and some vegetation attributes were measured at the watershed scale in 30 parcels of land which were separated into 15 fire-affected (burned) forests and 15 original (unburned) forests adjacent to the burned sites. The soil erodibility factor and splash erosion were also determined at the micro-plot scale within each burned and unburned site.

Furthermore, soil sampling and infiltration studies were carried out at 80 other sites, as well as the 30 burned and unburned sites, (a total of 110 points) to create a map of the soil erodibility factor at the regional scale. Maps of topography, rainfall, and cover-management were also determined for the study area. The maps of erosion risk and erosion risk potential were finally prepared for the study area using the Revised Universal Soil Loss Equation (RUSLE) procedure. Results indicated that destruction of the protective cover of forested areas by fire had significant effects on splash erosion and the soil erodibility factor at the micro-plot scale and also on surface erosion, erosion risk, and erosion risk potential at the watershed scale. Moreover, the results showed that correlation coefficients between different variables at the micro-plot and watershed scales were positive and significant. Finally, assessment and monitoring of the erosion maps at the regional scale showed that the central and western parts of the study area were more susceptible to erosion compared with the western regions due to more intense crop-management, greater soil erodibility, and more rainfall. The relationships between erosion parameters and the most important vegetation attributes were also used to provide models with equations that were specific to the study region. The results of this paper can be useful for better understanding erosion processes at the micro-scale and macro-scale in any region having similar vegetation attributes to the forests of northern Iran.

A. Akbarzadeh · S. Ghorbani-Dashtaki (✉) ·
M. Naderi-Khorasgani
Department of Soil Science, Faculty of Agriculture, Shahrekord
University, Shahrekord 88186-34141, Iran
e-mail: ghorbani-sh@agr.sku.ac.ir

S. Ghorbani-Dashtaki
e-mail: shoja2002@yahoo.com

A. Akbarzadeh
e-mail: akbarzadehali22@yahoo.com

M. Naderi-Khorasgani
e-mail: khnaderi@yahoo.com

R. Kerry
Department of Geography, Brigham Young University, Provo, UT,
USA
e-mail: ruth_kerry@byu.edu

R. Taghizadeh-Mehrjardi
Faculty of Agriculture and Natural Resources, Ardakan
University, Ardakan 89516-56767, Iran
e-mail: rh_taghizade@yahoo.com

Keywords Erosion map · Parcel · RUSLE · Splash erosion · Fire damage

Introduction

The frequency and extent of fire occurrence have increased dramatically in the forests of northern Iran (near the southwestern regions of the Caspian Sea) in recent decades (Heydaripour 2013). The increase in fire risk in this region is generating considerable concern about a range of associated environmental problems, including flash flooding, declining water quality, debris flows, and landslides (Norouzi and Ramezanzpour 2012). The destruction of the protective cover of forests by fire can cause a significant decrease in soil cohesion and permeability (Brath et al. 2006; Eisenbies et al. 2007), resulting in enhanced erosion rates and surface runoff (Benavides-Solorio and MacDonald 2001; Larsen et al. 2009; Pierson et al. 2008; Providali et al. 2002; Robichaud 2000). Fire significantly changes vegetation attributes and soil quality and, therefore, can have a great impact on soil erosion processes, especially in mountainous areas with unstable and loose geologic materials (Moffet et al. 2007). Therefore, precise identification of the erosion-prone areas can help (e.g., Aiello et al. 2015; Asadi et al. 2011; Chen et al. 2011; Prasannakumar et al. 2011; Vrieling et al. 2008) overcome erosion problems caused by fire. Many investigations have been conducted using different variables and analytical methods with this aim (e.g., Bargiel et al. 2013; Begueria 2006; Conoscenti et al. 2008; Mosbahi et al. 2013; Mueller et al. 2005; Tang et al. 2015; Xu et al. 2013).

Erosion processes are controlled by several variables including, rainfall intensity, landscape characteristics, soil particle features, ground cover, and land use. The process of soil loss by water begins with the separation and transport of soil particles by the force of impact of raindrops at the small scale. However, splash erosion is generally supposed to be only the first phase in the soil loss process. In the second phase, which is named surface erosion, a thin sheet of earth may be removed from the topsoil. In the next step, rill erosion, surface streams start to concentrate on steep land. In the final stages, gully and channel erosions occur when the power of runoff increases within rills. Therefore, to reduce soil loss by water, it is necessary to measure erosion at various scales ranging from the micro-scale to the macro-scale (Vrieling 2006). Scale is perhaps the most important issue in soil erosion studies because variables affecting soil loss are dependent on scale. In addition, knowing the scale at which soil loss takes place is

essential for erosion model development. Furthermore, the scale can influence the strategies and procedures used in soil conservation decisions (Cotler and Ortega-Larrocea 2006).

There are many works in the literature which are related to soil loss studies at small scales. However, the validity of expanding the results of these studies to broader scales is uncertain (Khalili Moghadam et al. 2015). Thus, it is important to assess erosion processes at a variety of scales from small to large scale (Zhao et al. 2013). Soil erosion studies at small scales such as a micro-plot or plot scale may use the direct measurement of rain splash erosion rate generated by a rainfall simulator (Khalili Moghadam et al. 2015) or the direct monitoring of erosion rates by pins and bars (Stoffel et al. 2013). Rain splash erosion is associated with the soil erodibility factor (Rezaie Pasha et al. 2012).

There are several empirically based methods in science for estimating erosion risk at the landscape scale (Renschler and Harbor 2002). Such empirical models predict soil loss by incorporating a pre-determined series of variables, measured using common methods. The most commonly used empirical model for estimating sheet and rill soil erosion by rain is the Universal Soil Loss Equation (USLE) and its revised version, the Revised Universal Soil Loss Equation (RUSLE) (Eisazadeh et al. 2012). Both the USLE and RUSLE calculate the average yearly soil loss anticipated on a hillside using six factors. These include rainfall (R), soil erodibility (K), slope length (L), slope steepness (S), crop management (C), and erosion control practices (P). In both models, the R-factor is computed on the basis of precipitation power, the K-factor is a function of soil characteristics, the LS-factor shows the topographic characteristics, the C-factor is a function of ground cover, and the P-factor relates to any erosion management practice. However, major modifications to the exact algorithms used to compute the factor were made in the RUSLE (Renard et al. 1991).

Although the RUSLE is an empirical model, erosion studies at a large scale such as a watershed or regional scale may also be performed with the combination of remote sensing (RS), geographical information systems (GIS), and RUSLE techniques (Prasannakumar et al. 2011). Remote sensing provides information sampled in a uniform way from wide areas with a systematic repeat times and is consequently able to significantly assist large scale soil loss evaluation (Alexakis et al. 2013; Kumar et al. 2014; Rahman et al. 2009; Vrieling

2006). For these reasons, the combined application of RS, GIS, and RUSLE methods make soil loss prediction possible at a reasonable expense and greater accuracy than using RUSLE alone. This is especially true at the watershed scale, which corresponds more to the requirements of management of soil and water resources than micro-scale studies (Prasannakumar et al. 2011). In recent years, digital mapping techniques have been considered an efficient approach to study different soil properties at large scales (Brevik et al. 2016). Mapping soil properties by digital techniques includes the acquisition of soil sampling and observation of associated pedological factors which are able to indicate how the soil developed (McBratney et al. 2003). The synchronization of this information collected by new procedures can be a convenient and low-cost alternative to traditional costly techniques (Taghizadeh-Mehrjardi et al. 2014). Methods used in digital mapping include logistic regression (Jafari et al. 2012), artificial neural networks (McBratney et al. 2003), machine learning systems (Lacoste et al. 2011), and regression tree analysis (Taghizadeh-Mehrjardi et al. 2014). Digital mapping of the soil erodibility factor using regression tree analysis can be a reliable approach to large scale erosion assessment.

Various natural physical features or landforms (lithology and morphology) covered with a variety of plant species may have different soil characteristics. In addition, the active erosion processes working on each specific landform may be different from other landforms. Therefore, land use/cover and geomorphology affect the rate of soil loss caused by the erosive forces of precipitation and surface overland flow (Cotler and Ortega-Larrocea 2006; Khalili Moghadam et al. 2015). The use of land cover and landforms as separate factors will increase the ability to better differentiate soil genesis and development characteristics in the natural environment (Cotler and Ortega-Larrocea 2006). Hence, the proper separation of land units having uniform and homogenous properties can have an important role in land degradation studies. Geo-pedological methods, which are based on landscape analysis, are considered to be a reliable and efficient technique for identifying different land units (subland units) with reasonable homogeneity (Anjos et al. 1998; Zink 1989). Such approaches can be very useful in land degradation studies, especially when investigating soil loss caused by destruction of vegetation cover by fire and changes in landforms.

Complete information about erosion processes at different scales within fire-affected regions and their surrounding environment, which are considered areas susceptible to the land degradation, could greatly improve judgments about erosion risk. In addition, assessing soil erosion risk in fire-affected regions at different scales could be critical for soil conservation plans on a broader scale (Heydaripour 2013). Hence, the main objective of this study was the measurement of soil erosion at micro-scale and macro-scale using laboratory experiments, field work, and remote sensing methods within a critical region of fire-affected forests on the southwestern coast of the Caspian Sea in the Guilan province of northern Iran.

Materials and methods

Study area description

The study area is located in the south western coastal zone of the Caspian Sea in northern Iran, with latitude between 38° 19' and 38° 23' N and longitude between 48° 43' and 48° 50' E (Fig. 1). The region belongs to the Kanroud forests of Astara district with an area of 21.54 km². The climate is classified as temperate humid Mediterranean based on the Emberger climatic classification system. The mean annual temperature and precipitation are 13.1 °C and 914 mm, respectively. The soil moisture and temperature regimes are Udic and Mesic, respectively.

Identification of the study sites

Figure 2 shows the methodology followed in this research as a flowchart. First, the map of the subland units of the Kanroud region was extracted from available literature (Abbasian 2012) as a raster image. This map was produced using geopedological methods (Anjos et al. 1998; Zink 1989). The approach used had a hierarchical structure involving field visits, interpretation of aerial photographs, satellite images, and any schematic maps, including geology, topography, soil, and land cover (vegetation) maps to separate the area into land units. In the method, all of the landforms in the study area were identified and separated by field visits and interpretation of aerial photographs and satellite imagery. The landform information was stored as a data layer in the Aeronautical Reconnaissance Coverage

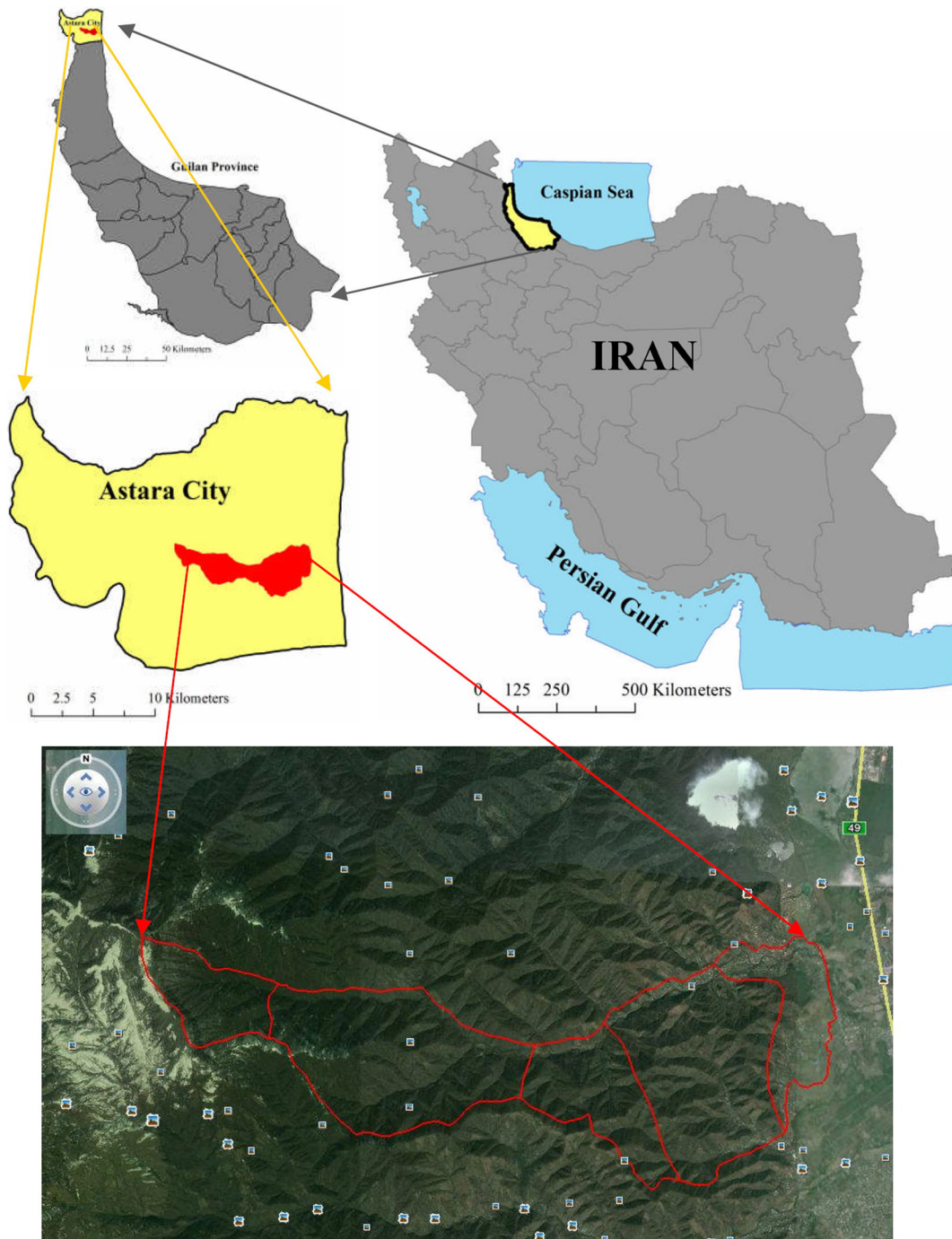


Fig. 1 Location of the study area and subland units on a Google Earth map

Geographic Information System (ArcGIS) environment (ESRI 2006). Similarly, the lithologic (geology) units and soil classes were extracted from available maps and were stored in the ArcGIS environment as the second and third data layers, respectively. The soils were

classified according to *Soil Taxonomy* (Soil Survey Staff 2014) and the *World Reference Base for Soil Resources* (World Soil Resources Reports 2014). Soil limitations were determined based on the Iranian Land Classification Guide (Mahler 1979). The information on

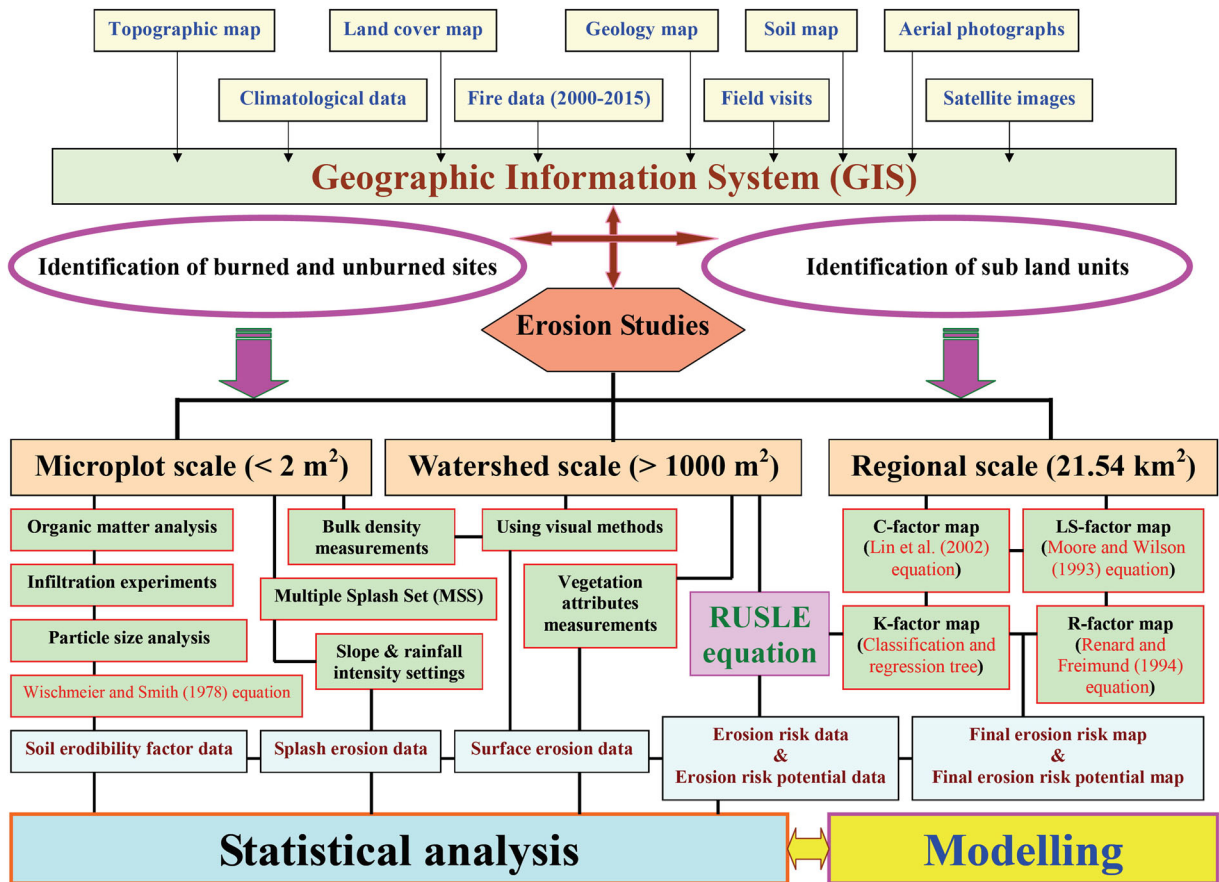


Fig. 2 Flowchart showing the methodology followed in the study

land cover and topography was also inserted into the data set. Finally, a map of land units was produced by combining different data layers in the ArcGIS environment. The land use for the whole study area was forest, and consequently, the land cover did not have a great influence on the land separation method. Therefore, only one land unit with forest land use was identified in the study area. This was then divided into five subland units to separate landforms and the soil main groups (Fig. 3 and Table 1). Over the years, many fires have occurred in the Kanroud region and therefore, this region is known as a critical area. After careful field visits to some fire-affected (burned) forests in the region, three burned sites were selected per subland unit (15 sites in total). Some properties of the burned sites are presented in Table 2. In this table, the intensity of fire was determined using the method proposed by Robichaud (2000). Table 2 also shows the interval of time between the occurrence of fire and commencement of experiments on 1 April 2015 (basis time) for each

site. Adjacent to the fire-affected forests, some unburned forests were selected as control site. The burned and unburned (control) sites had similar conditions in terms of topography, vegetation, and factors influencing soil properties. Figure 4 shows a burned site and its adjacent unburned site in one of the forests of the study area.

A parcel/large plot with specific shape and size was delimited within each burned and unburned site using existing natural features in the forest such as ridges, valleys, and roads. The boundaries of 30 parcels were determined by surveying equipment which included a laser meter, tape measure, range pole, level rod, theodolite, and clinometer. The area of each parcel within the limits of burned and unburned sites is given in Table 3. The 30 parcels were more than 1000 m², and therefore, the studies could be performed at the watershed scale. Parcels located in subland units 1.1.1, 2.1.1, 1.1.2, 2.1.2, and 2.1.3 were entitled A, B, C, D, and E, respectively (Fig. 3). The letters O and F, which accompany the letters A, B, C, D, and E, in each parcel name are related

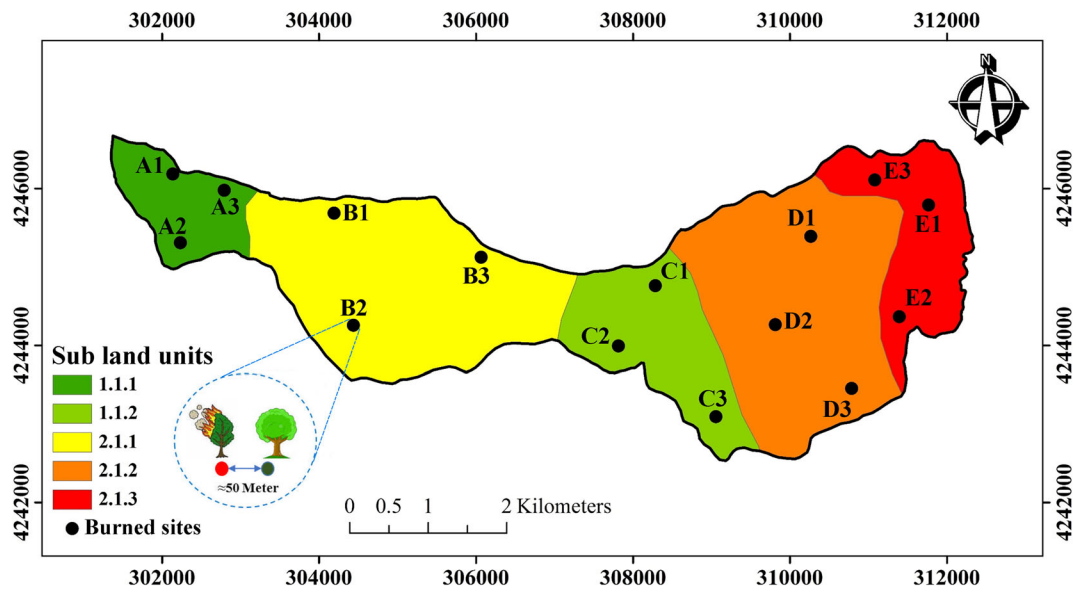


Fig. 3 Map of subland units in the study area along with zones disturbed by fire

to whether the site was fire-affected (F) or in its original condition (O) being a control site (Table 3).

Forest biometry

In each parcel, all living tall and small tree species that had a diameter at breast height of >7.5 cm (the counting limit) were measured using the 100% inventory or full callipering method. In this method, the diameter at breast height of each tree that was more than the counting limit was measured in diameter classes of 1 cm. The number of trees per hectare was measured by calculating the number of trees in each parcel and dividing this by the parcel area. The percentage of tree canopy cover was determined using the measurement of canopy area by inventory of two small and large diameters of canopy. The diameter at breast height of trees was determined by means of a caliper. The full height of trees was determined using a Suunto clinometer (PM5/360PC) and an ultrasonic Vertex III hypsometer. The thickness of surface litter (dead leaves) was randomly measured at several points within each parcel (Namiranian 2007; Zobeiry 2005 and 2007). The measurements for each parameter were reported as an average of that parameter for each parcel (Table 3). The average age of trees in each parcel (Table 3) was determined using several methods: (a) consulting experts in silviculture and forestry and local residents; (b) available literature about the dates various species were planted in

Guilan province (Gorji Bahri et al. 2012; Mosayeb Neghad et al. 2007; Sadegh 2011); (c) examining relationships between age, height, and diameter of special tree species (Mirabdollahi Shamsi et al. 2013); (d) counting the growth rings when a fallen trunk of a tree was found in the area (Mohammadi et al. 2012); and (e) dendrochronological analysis of selected trees in each parcel using an increment borer. To keep tree damage to a minimum, this method was only used for a small number of trees (Devall et al. 1995; Banj Shafiei et al. 2009).

Erosion measurement at the watershed scale

The surface erosion in each parcel was identified and measured using a visual index method. Soil accumulation around plants, stones, fences, and barriers was carefully investigated (Sadeghi 1995). The height of soil loss (in mm) was measured near plants, stones, fences, barriers, and roots of trees at several random points within each parcel. Finally, the surface erosion was reported as an average for each parcel in millimeters per hectare. According to the available literature and the aerial photographs, all parcels, burned and unburned, were forested in the past years and surface erosion ($\text{mm ha}^{-1} \text{ year}^{-1}$) was determined using the average age of trees in each parcel. The total mass of surface erosion ($\text{t ha}^{-1} \text{ year}^{-1}$) was measured for each site using soil surface bulk density (Sadeghi et al. 2006).

Table 1 Key to the map of subland units for the study area

Subland unit	Physical properties	Parent materials	Vegetation attributes	Soil properties	Soil classification
1.1.1 and 1.1.2	Slightly tall mountains to relatively tall hills; very steep slopes; very rocky outcrops and having rocky walls	Andesite tuffs	Forest species with intense density; litter thickness of 2 to 5 cm	Nondeveloped soils; low depth (maximum depth of 48 cm); stony (15–35%); profile type: AC to A(B)C; texture in surface and subsurface is loam; pH values 5.5–6.5; structure in surface is coarse granular and in subsurface is without clear shape	<i>Lithic Udorthents</i> ^a ; <i>Dystric Leptosols</i> ^b
2.1.1 and 2.1.2	Slightly tall hills to low hills; slightly steep slopes; slightly rocky outcrops	Tuffs, andesite, and basalt	Forest species with intense to moderate density; litter thickness of 2 to 6 cm	Slightly developed to developed soils; low depth (maximum depth of 55 cm); without stones to the depth of 30 cm; profile type: A(B)C to ABC; texture in surface is loam and in subsurface is loam to clay loam; pH values 5.2–6.1; structure in surface is coarse to medium granular and in subsurface is polyhedron	<i>Lithic Hapudolls</i> ^a ; <i>Leptic Phaeozems</i> ^b
2.1.3	Low hills; low slopes; rarely having rocky walls	Siltstones and sandstones	Forest species with moderate to low density; litter thickness of 1 to 4 cm	Developed soils; slightly high depth (maximum depth of 85 cm); without stones to the depth of 75 cm; profile type: ABC; texture in surface is loam and in subsurface is clay loam; pH values 4.9–5.6; structure in surface is medium to fine granular and in subsurface is polyhedron to prismatic	<i>Typic Argiudolls</i> ^a ; <i>Haplic Luvisols</i> ^b

^a Soil type classification based on *Soil Taxonomy* (Soil Survey Staff 2014)

^b Soil type classification based on the *World Reference Base for Soil Resources* (World Soil Resources Reports 2014)

Table 2 Some properties of the burned sites in the study area

Site	Elevation (m)	Slope (%)	Average annual precipitation (mm)	Average annual temperature (°C)	Fire type	Fire severity	Fire area (m ²)	Interval to basis time (years)
A1	815	36.62	826	12.5	Surface	Low	5000	9.17
A2	997	71.75	740	11.75	Surface	Low	8000	8.33
A3	603	35.07	938	13.25	Surface	Low	6000	5.5
B1	356	23.61	1087	14	Canopy	High	50,000	2.58
B2	542	47.10	973	13.75	Trunk	High	10,000	5.5
B3	159	36.11	1224	14.75	Surface	Low	6000	6.5
C1	105	45.52	1264	15	Canopy	High	33,000	1.33
C2	293	66.59	1129	14.5	Canopy	High	30,000	2.5
C3	320	23.59	1111	14.5	Trunk	Low	7000	6.33
D1	171	44.64	1215	14.75	Canopy	High	20,000	5.5
D2	144	30.84	1235	15	Canopy	High	21,000	3.58
D3	29	18.69	1323	15.5	Canopy	High	15,000	4.92
E1	32	17.54	1321	15.5	Surface	Low	9500	9.42
E2	26	27.28	1325	15.75	Surface	Low	7500	6.42
E3	8	13.28	1340	15.5	Canopy	High	27,500	4.17

Experimental design and sample collection

To study the effects of fire on soil erosion parameters, 30 sites were chosen of two types, 15 fire-affected and 15 controls that had not been burned. There were three replicates for each type of site and relevant experiments were conducted on each repeat. This resulted in soil bulk density, permeability of the soil profile, and splash erosion being measured at a total of 90 points, and 90 soil samples were collected for laboratory analyses. In addition, soil sampling and infiltration studies were carried

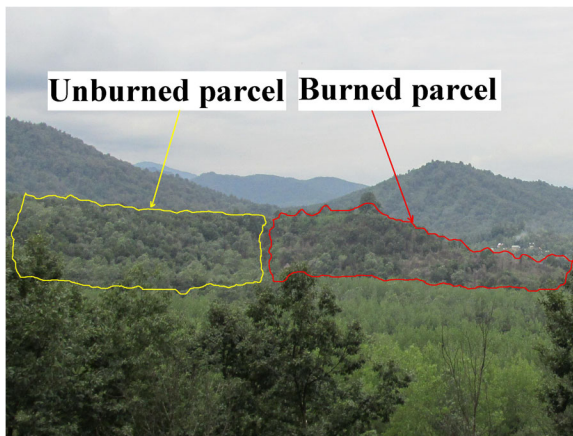


Fig. 4 A distant view from one of the burned sites towards its adjacent unburned site in the study area

out at 80 other sites, in addition to the 30 burned and unburned sites (110 points in total), to provide a map for the soil erodibility factor at the regional scale (Fig. 5). Before performing the experiments and sampling, any litter and ash were carefully removed from the soil surface by brushing based on the precedent set in similar studies carried out in forests (Zavala et al. 2010). Topsoil samples were taken at a depth of 0–15 cm using a cylinder and the air-dried <2 mm fraction used for physico-chemical laboratory analysis.

Field experiments and laboratory analysis

Topsoil bulk density was measured in the field using the cylinder technique (Blake and Hartge 1986). Soil permeability was evaluated in the field according to the final infiltration rate by measuring one-dimensional water flow into the soil per unit time using a double-ring infiltrometer (Bauwer 1986). The soil structure code and profile permeability class to estimate the soil erodibility factor (K-factor) were extracted from the *National Soils Handbook, No. 430* (USDA 1983). In the laboratory, particle size distribution of the soils was determined by sieving and sedimentation (Gee and Bauder 1986) and the organic matter content was calculated using the Walkley-Black method (Nelson and Sommers 1996). Soil splash erosion was measured in the laboratory using a multiple splash set (MSS) apparatus (Fig. 6).

Table 3 Some vegetation attributes and area (size) of parcels at the watershed scale

Parcel name	Parcel area (m ²)	Number of trees per hectare (trees)	Height of trees (m)	Diameter at breast height of trees (cm)	Canopy cover of trees (%)	Thickness of surface litter (cm)	Age of trees (years)
AO1	3900	402.6	14.5	20.9	68	4.6	90
AF1	3225	179.8	15.8	21.7	51	3.4	
AO2	2800	417.9	14.3	21.4	71	4.8	90
AF2	3050	180.3	16.0	22.7	50	2.9	
AO3	3500	388.6	14.1	20.6	68	4.8	85
AF3	2555	101.8	16.2	25.3	41	2.4	
BO1	3775	360.3	13.1	19.2	63	4.3	80
BF1	4025	19.9	20.0	30.5	15	0.0	
BO2	2900	379.3	13.9	20.5	66	4.5	80
BF2	3100	77.4	17.9	26.0	36	2.0	
BO3	4225	343.2	12.7	18.5	62	4.0	70
BF3	3750	112.0	14.4	22.0	42	2.7	
CO1	9125	321.1	11.2	17.9	60	4.0	60
CF1	7450	28.2	17.2	26.7	15	0.0	
CO2	4875	344.6	11.5	18.5	62	4.1	70
CF2	5300	34.0	16.6	27.9	13	0.0	
CO3	4850	350.5	12.8	18.9	63	4.3	75
CF3	3125	96.0	16.6	22.9	37	2.0	
DO1	6200	282.3	10.8	17.4	58	3.7	60
DF1	6825	74.7	14.3	22.8	34	1.8	
DO2	5025	300.5	13.2	19.0	57	3.8	35
DF2	4575	37.2	19.0	28.3	19	1.0	
DO3	7625	254.4	9.1	15.8	57	3.5	55
DF3	6650	58.6	12.0	22.6	26	1.2	
EO1	4550	219.8	8.6	14.3	54	3.3	50
EF1	5150	217.5	8.8	15.0	51	3.5	
EO2	6225	141.4	8.2	12.7	45	3.0	45
EF2	4400	109.1	8.9	14.5	42	2.6	
EO3	6750	69.6	6.0	12.3	33	1.5	45
EF3	7075	53.7	8.3	17.2	23	1.2	

This device is composed of three different systems, including rainfall simulator, slope regulator, and soil sample swirl. The rainfall simulator system includes an electric pump, telescopic tubes, and control valve suppliers for water flow and a nozzle. The nozzle framework diameter was designed to be 15 cm to create a complete overlap with the soil samples inside the sampling cylinder. The slope regulator provides the intended slope and necessary angle for running the experiments. The soil sample swirl system has its rotation energy supplied by an electromotor and is designed to cause splashing at a fixed point. This apparatus also consists of two cylinders, including a main cylinder with a diameter and height of 30 cm and a core sample cylinder with a diameter and height of 10 cm. The splash erosion caused by simulated rainfall on the core sample is collected by the main

cylinder. The main cylinder is divided into two parts: an upslope section and a downslope section. Hence, the amount of splash erosion in upslope and downslope directions can be measured separately. After drying and weighting of the particles splashed into the upper and lower parts of the main cylinder, the splash erosion rate was measured using the following formula (Eq. 1):

$$St = \frac{Su + Sd}{T \times A} \tag{1}$$

where *St* is the splash erosion rate (g min⁻¹ m⁻²), *Su* is the soil splashed upslope (g), *Sd* is the soil splashed downslope (g), *A* is the soil core sample area (m²), and *T* is the period of drop (min) (Khalili Moghadam et al. 2015). In the present investigation, soil splash erosion was calculated for each sample under two different slopes (5 and

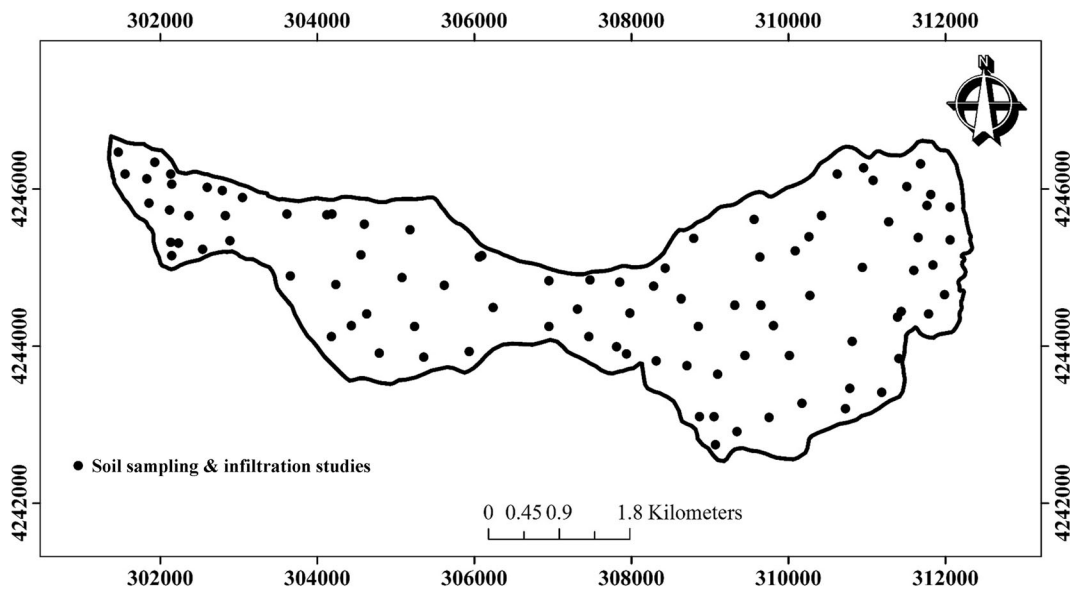


Fig. 5 The location of soil sampling points (110) and infiltration studies at the regional scale

40%) for 30 min of rainfall with an intensity of 50 mm h⁻¹. The rainfall intensity of 50 mm h⁻¹ is the

Drop-former chamber

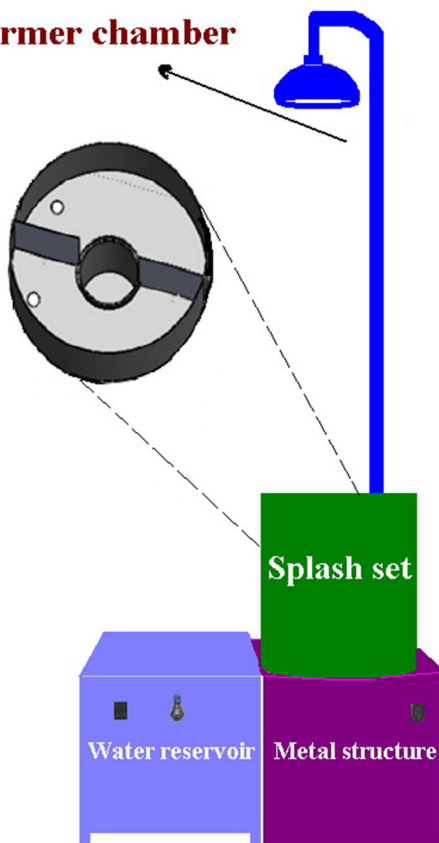


Fig. 6 Setup of the multiple splash set (MSS)

maximum rainfall intensity for the study area that occurred in 60 min with a return period of 10 years. This maximum rainfall intensity was determined from precipitation data for 17 climatological, synoptic, and rainfall stations located around the study area using the model (Eq. 2) proposed by Ghahraman and Abkhezr (2004).

$$R_{60}^{10} = e^{0.291} (R)^{0.694} \tag{2}$$

where R is the mean maximum daily rainfall (mm).

Erosion estimation

The RUSLE model (Eq. 3) was used to estimate the soil erosion in burned and control sites.

$$A = R \times K \times LS \times C \times P \tag{3}$$

where A is the soil loss per unit of area per unit of time (t ha⁻¹ year⁻¹) caused by sheet and rill erosion, R is the rainfall erosivity factor (MJ mm h⁻¹ ha⁻¹ year⁻¹), K is the soil erodibility factor (t h MJ⁻¹ mm⁻¹), LS is the slope length and steepness factor (dimensionless), C is the cover-management factor (dimensionless), and P is the support practice factor (dimensionless).

The K -factor was calculated using the model (Eq. 4) proposed by Wischmeier and Smith (1978).

$$100K = 2.1 \times 10^{-4} \times M^{1.14} \times (12-OM) + 3.25 \times (S-2) + 2.5 \times (P-3) \tag{4}$$

where K is the soil erodibility factor with US customary units $(100 \text{ acre ft. tonf in})^{-1}$, M is $[(100 - \% \text{ clay}) \times (\% \text{ very fine sand} + \% \text{ silt})]$, OM is the organic matter (%), S is the soil structure code, and P is the profile permeability class. To convert the K -factor units from US customary units into SI units, all the K -factor values were divided by 7.593. The K -factor map (Fig. 7) with a grid resolution of 90 by 90 m for the study area was prepared, according to classification and regression tree analysis (Breiman et al. 1984) through K -factor data related to 110 points (Fig. 5) using Cubist software (Quinlan 2001).

The R -factor map (Fig. 8) with a grid resolution of 90 by 90 m was calculated based on ordinary kriging method in the ArcGIS environment. The map was prepared using the modified Fournier index (Eq. 5) and precipitation data provided from 17 climatological, synoptic, and rainfall stations located around the study area using models (Eqs. 6 and 7) defined by Renard and Freimund (1994).

$$F = \frac{\sum_{i=1}^{12} P_i^2}{12 \sum_{i=1}^{12} P} \tag{5}$$

$$R = \frac{0.07397 F^{1.847}}{17.2}, \text{ when } F < 55\text{mm} \tag{6}$$

$$R = \frac{95.77 - 6.081 F + 0.4770 F^2}{17.2}, \text{ when } F \geq 55\text{mm} \tag{7}$$

where F is the modified Fournier index, R is the rainfall erosivity factor, P_i is the monthly precipitation (mm), and P is the yearly precipitation (mm).

The LS -factor map (Fig. 9) was determined by a model (Eq. 8) presented by Moore and Wilson (1992).

$$LS = 1.4 \left[\frac{As}{22.13} \right]^{0.4} \left[\frac{\text{Sin}B}{0.0896} \right]^{1.3} \tag{8}$$

where LS is the slope length and steepness factor, As is the unit contributing area (m) and B is the slope (degrees). A digital elevation model (DEM) with a grid resolution of 90 by 90 m (National Cartographic Center 2010) was used to determine the LS -factor. The maps of slope, flow direction, and flow accumulation were prepared in the ArcGIS environment using its spatial analyst function to derive the As and B values.

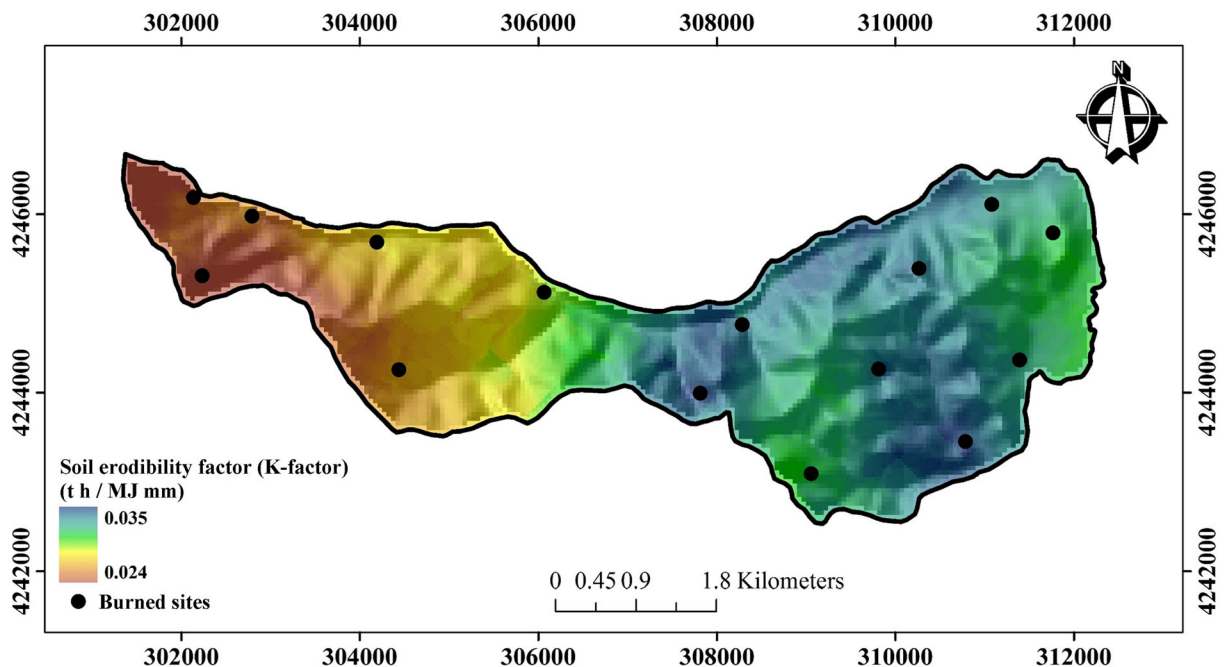


Fig. 7 Spatial distribution of the soil erodibility factor (K -factor) over the study area

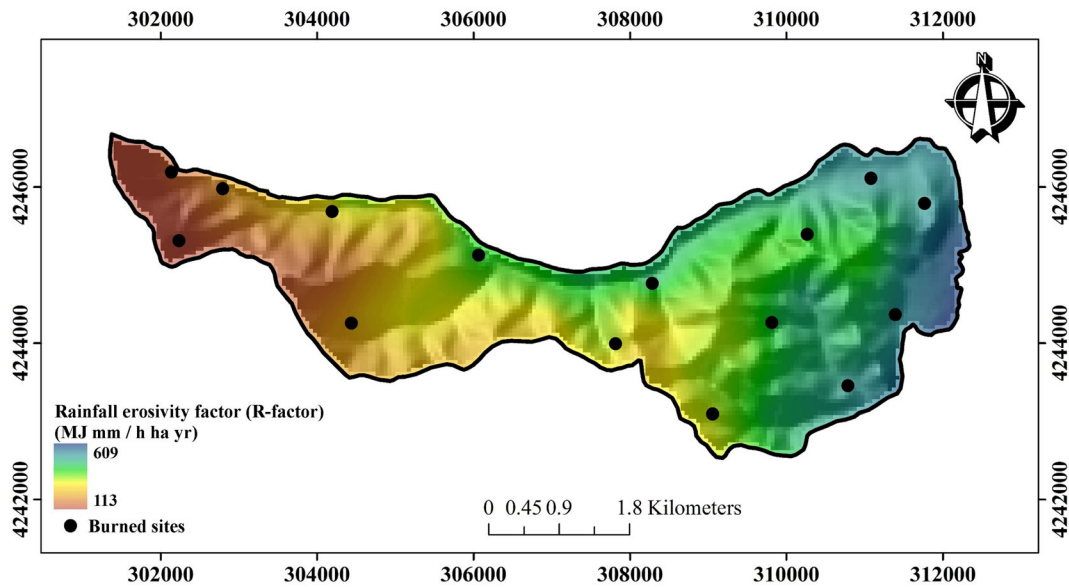


Fig. 8 Spatial distribution of the rainfall erosivity factor (*R-factor*) over the study area

Band four (Red) and band five (NIR) of Landsat 8 images from 2015 were used to calculate the normalized difference vegetation index (NDVI) for the study area using ERDAS Imagine (LEICA Geosystems 2003) with the formula (Eq. 9) expressed by Karaburun (2010):

$$NDVI = \frac{NIR - Red}{NIR + Red} \tag{9}$$

As forest observations and field experiments were conducted in the spring and summer, Landsat 8 images from these seasons were used to calculate NDVI. Finally, after testing some different C-factor models presented in the scientific literature (de Jong et al. 1998; Van der Knijff et al. 1999), the formula (Eq. 10) reported by Lin et al. (2002) was chosen to determine the C-factor map (Fig. 10) with a grid resolution of 90 by 90 m using ERDAS Imagine.

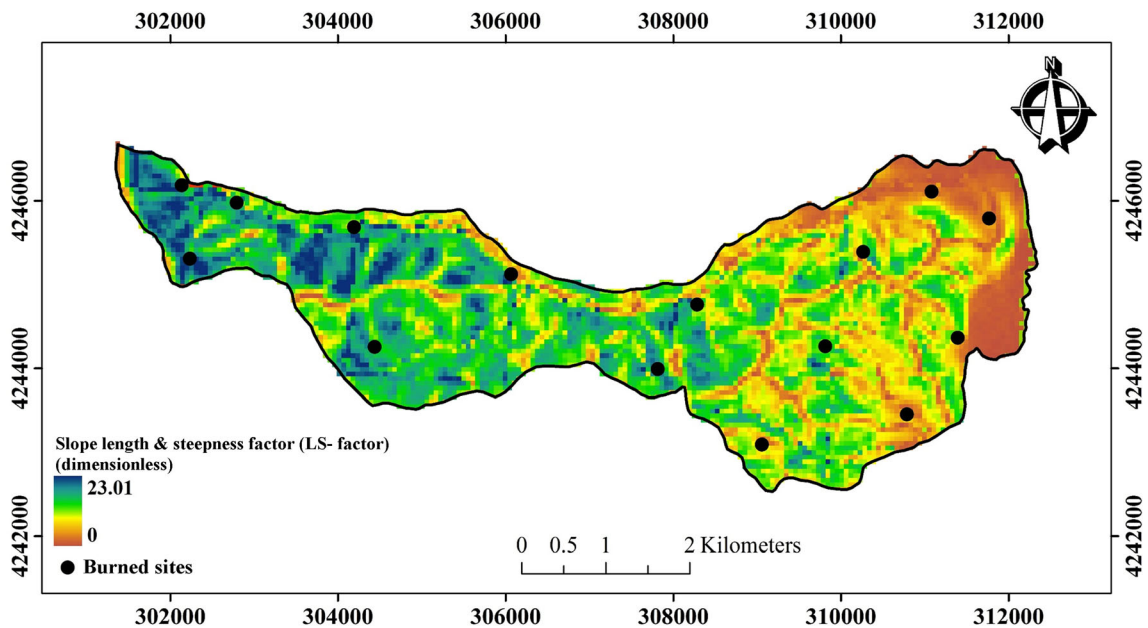


Fig. 9 Spatial distribution of the slope length and steepness factor (*LS-factor*) over the study area

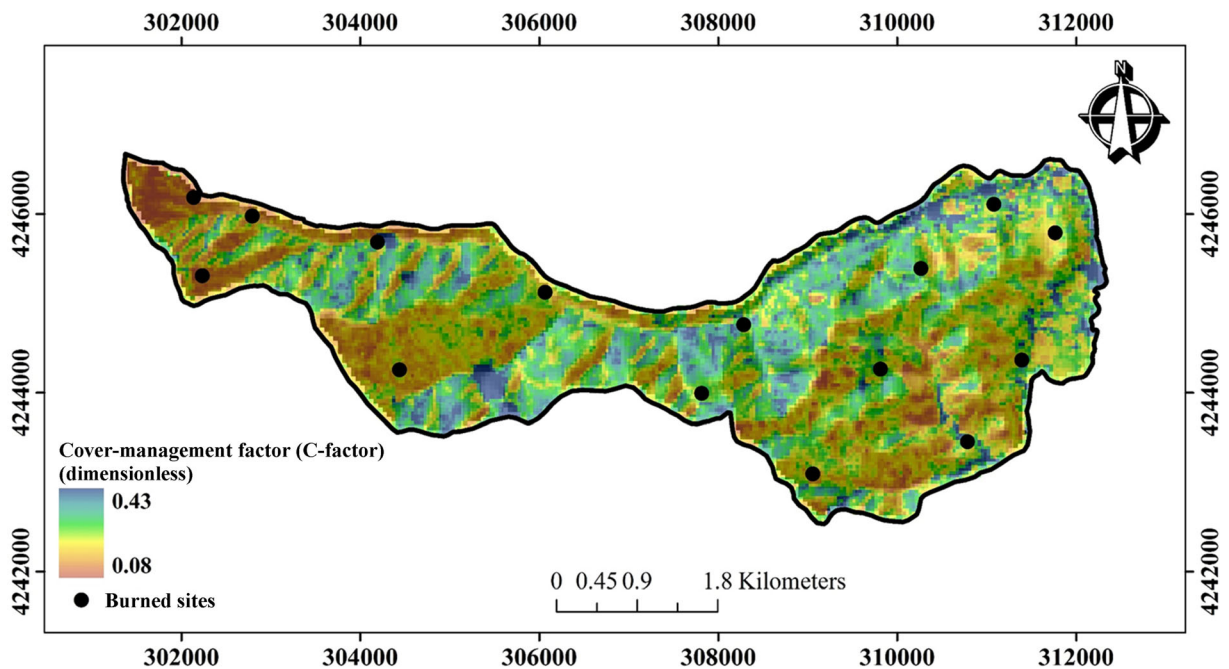


Fig. 10 Spatial distribution of the cover-management factor (*C-factor*) over the study area

$$C = \left(\frac{1 - NDVI}{2} \right)^{1 + NDVI} \tag{10}$$

The study area was located in a forest region, and hence, there were no protective operations such as contour cultivation, strip cropping, and terracing. Consequently, the support practice factor (P-factor) was considered one for the whole study area. The map of erosion risk (Fig. 11) was finally prepared for the study area by combining (multiplying) all factors ($K \times R \times LS \times C \times P$) in the ArcGIS environment using the RUSLE procedure. Also, to study the role of the complete destruction of forest cover in increasing erosion risk in the study area, a map was created by eliminating the C-factor and combining other remaining factors ($K \times R \times LS \times P$) (Fig. 12). All the maps were created in a coordinate system of WGS_1984_UTM_Zone_39N.

Statistical analysis

A split-plot spatial design with 30 burned and unburned (control) sites as the treatments was selected to analyze the extracted data. Statistical Package for the Social Sciences (SPSS) software (SPSS 1999) was used to perform the statistical analysis. The analysis of variance (ANOVA) tests were carried out using the general linear

model (GLM) method under the repeated measures define factors (RMDF) procedure to confirm whether there were significant variations in erosion parameters among the five subland units (between subjects) and also within burned and control sites (within subjects). Mean comparisons were performed for burned and control sites in each unique subland unit using the paired-samples *T* test at the 0.05 probability level. Step-wise regression was used to recognize the most sensitive factors for estimating the erosion parameters using multiple linear regression (MLR).

Results and discussion

The result of ANOVA showed that the soil erodibility factor and splash erosion (for 5 and 40% slopes) were significantly different ($p < 0.01$) between subland units at the micro-plot scale (Table 4). In contrast, there was no significant difference (at $p = 0.05$) in surface erosion, erosion risk, and erosion risk potential between subland units at the watershed scale (Table 5). However, all erosion parameters at the micro-plot and watershed scales showed a significant difference ($p < 0.01$) within subland units between burned and control sites (Tables 4 and 5).

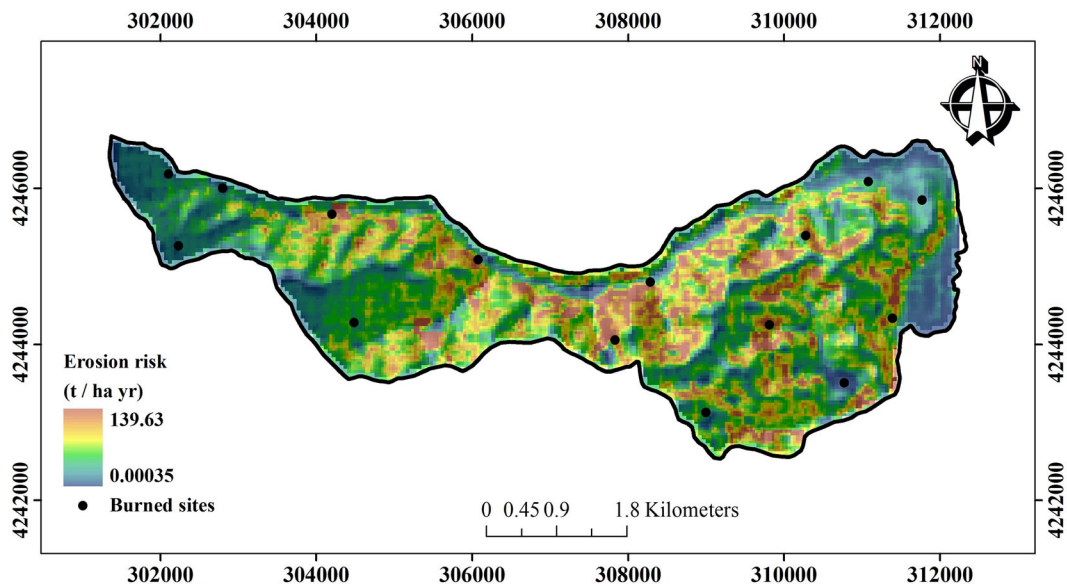


Fig. 11 Spatial distribution of erosion risk over the study area

Comparison of the average values showed that splash erosion for 5% slopes was significantly ($p < 0.05$) greater at burned rather than control sites in all (A–E) subland units at the micro-plot scale. In addition, splash erosion for 40% slopes as well as the soil erodibility factor in four subland units (A–D) in burned areas was significantly greater ($p < 0.05$) than at the

unburned sites at the micro-plot scale. The results also showed that an increase in slope inclination from 5 to 40% greatly enhanced the rate of splash erosion in all treatments. The lowest and highest values of splash erosion for 5% slopes were 2.95 and 4.36 $\text{g min}^{-1} \text{m}^{-2}$, respectively; while these values for 40% slopes were 32.51 and 43.98 $\text{g min}^{-1} \text{m}^{-2}$,

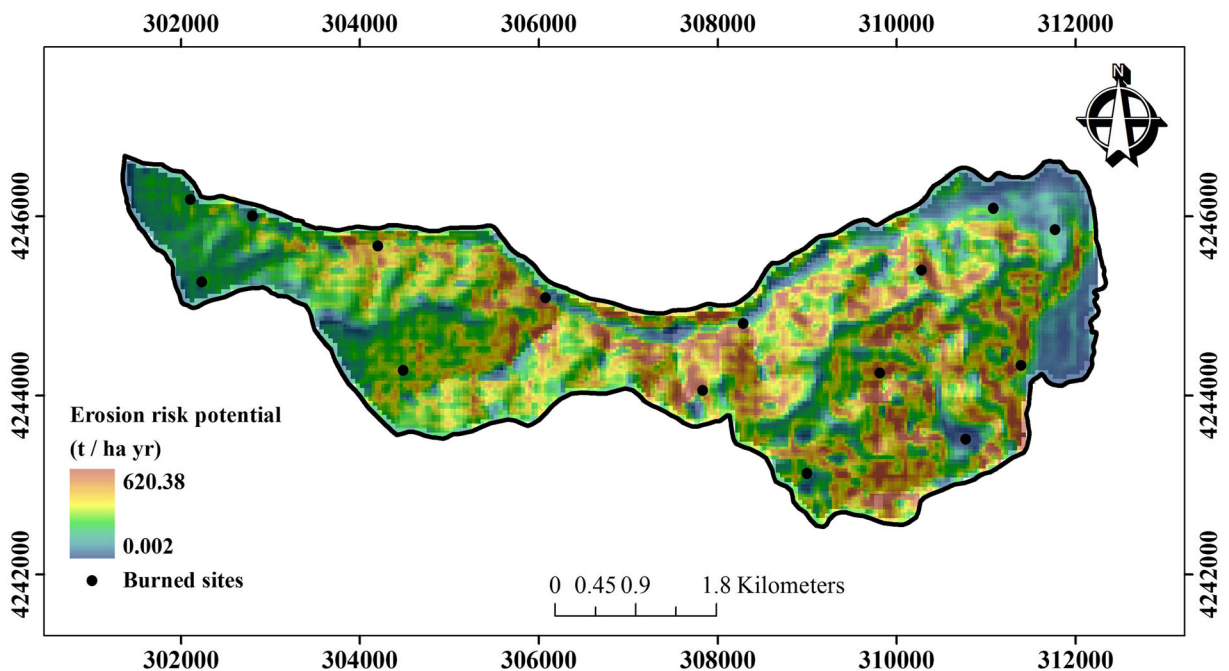


Fig. 12 Spatial distribution of erosion risk potential over the study area

Table 4 Analysis of variance of erosion parameters at the micro-plot scale

Source	Degrees of freedom	Mean squares (MS)		
		Splash erosion for 5% slopes	Splash erosion for 40% slopes	Soil erodibility factor
Between subjects	4	0.320**	22.975**	9.592×10^{-5} **
Within subjects	1	4.144**	226.930**	0.001**
Total	5	4.464	249.905	1.096×10^{-3}

*Significant at 0.05 probability level

**Significant at 0.01 probability level

respectively (Table 6). These results are supported by the findings of similar investigations. Baharloo et al. (2015) similarly reported that increasing slope inclination from 5° to 25° in fire-affected areas increased splash erosion by 15%. Yusefi et al. (2014) found that an increase in slope from 5 to 15% in deforested areas significantly enhanced splash erosion, and Gharemani et al. (2011) showed that an increase in the gradient of terrain features and a decrease in ground cover enhanced splash erosion in forests.

It has been shown that soil organic matter content has a high correlation with the soil erodibility factor (Wischmeier and Smith 1978). The soil organic matter content in areas with dense vegetation cover such as forests is naturally high. The high organic matter in soil helps bind soil particles and micro-aggregates into larger, stable aggregates. Soil organic matter also creates a hydrophobic coating around the aggregates, and this coating prevents or decreases the percolation of water into the aggregates. This may improve aggregate stability against internal stresses caused by rapid water uptake (wetting) and reduce aggregate breakdown and slaking (Quirk and Murray 1991). Consequently, in the present study, it is hypothesized that a decrease in soil organic matter content in fire-affected areas probably enhanced

the soil erodibility factor and splash erosion at the micro-plot scale.

The destruction of forest cover by fire may lead to greater rates of erosion compared with original forest at the watershed scale (Cotler and Ortega-Larrocea 2006). In the present study, the comparison of average values of surface erosion, erosion risk, and erosion risk potential at the watershed scale showed that all of the erosion parameters, except erosion risk in subland unit B, did not show a significant difference in any of the subland units within the burned and control treatments. However, the values of erosion parameters in burned treatments were more than unburned treatments for most of the sites at the watershed scale. Comparing the values obtained for erosion risk and erosion risk potential also revealed that with removal of the cover-management factor, the rate of erosion increased markedly (Table 7).

The process of soil erosion was evaluated at the micro-plot and watershed scales by development of a correlation matrix (Table 8) between variables related to two scales for the 30 studied sites. This two-scale soil erosion evaluation showed that there were significant ($p < 0.01$) positive correlations between the splash erosion (for 5 and 40% slopes) and the soil erodibility factor

Table 5 Analysis of variance of erosion parameters at the watershed scale

Source	Degrees of freedom	Mean squares (MS)		
		Surface erosion	Erosion risk	Erosion risk potential
Between subjects	4	295.722 n.s	385.253 n.s	4757.199 n.s
Within subjects	1	1657.336**	1882.426**	5579.033**
Total	5	1917.058	2267.679	10,336.232

n.s not significant

*Significant at 0.05 probability level

**Significant at 0.01 probability level

Table 6 Comparison of the average values of erosion parameters at the micro-plot scale

Site	Splash erosion for 5% slopes (g min ⁻¹ m ⁻²)	Splash erosion for 40% slopes (g min ⁻¹ m ⁻²)	Soil erodibility factor (t h MJ ⁻¹ mm ⁻¹)
AO	2.95 (0.10)a	32.51 (1.26)a	0.024 (0.002)a
AF	3.76 (0.19)b	39.35 (1.25)b	0.032 (0.002)b
BO	3.16 (0.11)a	34.95 (1.55)a	0.026 (0.001)a
BF	4.22 (0.17)b	42.43 (1.71)b	0.040 (0.004)b
CO	3.30 (0.10)a	35.97 (0.91)a	0.028 (0.001)a
CF	4.26 (0.10)b	42.85 (0.63)b	0.042 (0.001)b
DO	3.63 (0.25)a	38.69 (1.47)a	0.031 (0.001)a
DF	4.36 (0.08)b	43.98 (1.09)b	0.045 (0.003)b
EO	3.68 (0.23)a	38.90 (1.27)a	0.030 (0.002)a
EF	3.83 (0.22)b	39.91 (0.78)a	0.030 (0.002)a

Properties having different letters are significantly different at the 0.05 probability level. Numbers in parentheses are standard deviations

at the micro-plot scale and surface erosion, erosion risk, and erosion risk potential at the watershed scale. These positive correlations between variables from two scales of observation confirmed that erosion which begins at the micro-scale leads to soil loss at the macro-scale. Moreover, the correlation matrix shows that there were correlations between some vegetation attributes and erosion parameters at the micro-plot and watershed scales (Table 8). Therefore, as fire in forests changes vegetation attributes, there can probably be adverse effects on soil properties that enhance erosion rates (Cotler and Ortega-Larrocea 2006). Many studies have also confirmed the high correlation between vegetation cover and soil erosion (Battany and Grismer 2000; Wainwright et al. 2000; Vrieling et al. 2008).

Results at the regional scale showed that from the mountainous regions (west) to the flat regions (east) of the study area and approaching the Caspian Sea (Fig. 1 and Table 1), vegetation density decreased, while fine soil particles (soil silt and clay content) increased. Towards the eastern parts of the study area, human activities and grazing increased and, hence, disturbance of vegetation cover was enhanced, especially close to the residential areas. Consequently, points located in western parts of the study area had denser vegetation cover compared with points in eastern and central parts. Increase in soil organic matter content and decrease in soil fine fractions had a significant role in enhancing the detachability of particles and the soil erodibility factor (Wang et al. 2013).

Table 7 Comparison of the average values of erosion parameters at the watershed scale

Site	Surface erosion (t ha ⁻¹ year ⁻¹)	Erosion risk (t ha ⁻¹ year ⁻¹)	Erosion risk potential (t ha ⁻¹ year ⁻¹)
AO	3.02 (0.94)a	5.11 (1.55)a	3.02 (0.94)a
AF	10.53 (5.67)a	13.17 (6.43)a	10.53 (5.67)a
BO	4.02 (0.23)a	6.52 (0.41)a	4.02 (0.23)a
BF	21.44 (11.30)a	24.80 (11.7)a	21.44 (11.30)b
CO	8.36 (5.43)a	11.73 (7.32)a	8.36 (5.43)a
CF	40.16 (28.60)a	45.78 (32.03)a	40.16 (28.60)a
DO	6.90 (2.33)a	9.63 (3.48)a	6.90 (2.33)a
DF	23.74 (13.73)a	27.67 (15.46)a	23.74 (13.73)a
EO	7.43 (5.30)a	9.24 (6.71)a	7.43 (5.30)a
EF	8.20 (6.15)a	10.01 (7.36)a	8.20 (6.15)a

Properties having different letters are significantly different at the 0.05 probability level. Numbers in parentheses are standard deviations

Table 8 Pearson’s correlation coefficients among different variables at the micro-plot and watershed scales

	<i>No</i>	<i>He</i>	<i>Di</i>	<i>Ca</i>	<i>TL</i>	<i>Sp5</i>	<i>Sp40</i>	<i>K</i>	<i>SE</i>	<i>ER</i>	<i>ERP</i>
<i>No</i>	1										
<i>He</i>	-0.211 n.s	1									
<i>Di</i>	-0.380*	0.951**	1								
<i>Ca</i>	0.951**	-0.305 n.s	-0.505**	1							
<i>TL</i>	0.941**	-0.312 n.s	-0.513**	0.993**	1						
<i>Sp5</i>	-0.953**	0.294 n.s	0.467**	-0.928**	-0.919**	1					
<i>Sp40</i>	-0.929**	0.264 n.s	0.434*	-0.901**	-0.886**	0.982**	1				
<i>K</i>	-0.844**	0.510**	0.644**	-0.866**	-0.861**	0.928**	0.911**	1			
<i>SE</i>	-0.629**	0.533**	0.661**	-0.767**	-0.774**	0.668**	0.651**	0.733**	1		
<i>ER</i>	-0.606**	0.536**	0.658**	-0.744**	-0.751**	0.649**	0.633**	0.720**	0.999**	1	
<i>ERP</i>	-0.353 n.s	0.477**	0.541**	-0.476**	-0.475**	0.428*	0.426*	0.531**	0.879**	0.901**	1

No number of trees per hectare, *He* height of trees, *Di* diameter at breast height of trees, *Ca* canopy cover of trees, *TL* thickness of surface litter, *Sp5* splash erosion for 5% slopes, *Sp40* splash erosion for 40% slopes, *K* soil erodibility factor, *SE* surface erosion, *ER* erosion risk, *ERP* erosion risk potential, *n.s* not significant

*Significant at 0.05 probability level

**Significant at 0.01 probability level

Areas having rocky outcrops were abundant in the western part (mountainous regions) of the study area (Table 1). The soil erodibility factor in these areas was zero due to lack of soil (Asadi et al. 2011). Evaluation of the spatial distribution of the soil erodibility factor at the regional scale showed that from the western to the eastern regions of the study area, the soil erodibility factor increased from 0.024 to 0.035 t h MJ⁻¹ mm⁻¹ (Fig. 7). Results also showed that precipitation increased, and elevation and steepness decreased due to decreasing altitude (height above sea level) from west to east and approaching sea level (Table 2). Increase in precipitation will enhance the rainfall erosivity factor (Renard et al. 1991). Studying the spatial distribution of the rainfall erosivity factor at the regional scale revealed that from western to eastern regions of the study area the rainfall erosivity factor increased from 113 to 609 MJ mm h⁻¹ ha⁻¹ year⁻¹ (Fig. 8). The slope length and steepness factor at the regional scale was between 0 (in the east) and 23.01 (in the west). Therefore, the slope length and steepness factor decreases from the mountainous regions to the flat regions of the study area (Fig. 9). Decrease in vegetation cover density will increase the cover-management factor (Lin et al. 2002). Spatial distribution of the cover-management factor showed that its values ranged between 0.08 (high crop cover) and 0.43 (almost bare soil) over the study area. In general, the values of the cover-management factor in

central and eastern parts of the study area were less than in western parts (Fig. 10). Increase in the soil erodibility, rainfall erosivity, and cover-management factors can enhance the erosion risk in an area (Aiello et al. 2015). The map of the erosion risk (Fig. 11) showed that the estimated erosion values ranged between 0.00035 and 139.63 t ha⁻¹ year⁻¹. In addition, spatial distribution of the erosion risk over the study area illustrated that the central and western sections of the study area were more susceptible to erosion compared with the western regions because of larger values for the crop-management, soil erodibility, and rainfall factors. Despite higher values for the slope length and steepness factor in western parts, this factor did not increase the erosion risk in these regions by itself because of the lower values of other factors. Furthermore, the map of erosion risk potential (Fig. 12) revealed that elimination of the cover-management factor increased soil erosion by 620.38 t ha⁻¹ year⁻¹, and therefore, the important role of the vegetation cover in reducing soil loss over the study area is apparent from this map.

To develop model equations for estimating erosion parameters in the study area, multiple linear regression between the erosion parameters and the main vegetation variables was investigated using a step-wise approach. Table 9 shows 10 models for estimating erosion parameters at the micro-plot and watershed scales using vegetation attributes as the independent variables. Results

Table 9 Results of step-wise multiple linear regression for estimating erosion parameters

No.	Model	Linear regression equation	Standard error	R ²	F (sig)
1	1	$Sp5 = -0.003No + 4.392$	0.14797	0.909	279.485**
2	2	$Sp5 = -0.003No + 0.013Di + 4.100$	0.13967	0.922	159.057**
3	1	$Sp40 = -0.025No + 43.977$	1.38711	0.862	175.339**
4	1	$K = 0.0001Ca + 0.049$	0.000	0.750	84.031**
5	2	$K = 0.0001Ca + 0.001He + 0.040$	0.000	0.816	60.021**
6	1	$SE = -7.701TL + 35.173$	9.41744	0.599	41.912**
7	2	$SE = -5.873TL + 1.124Di + 6.989$	8.38350	0.694	30.610**
8	1	$ER = -8.266TL + 39.759$	10.8690	0.564	36.252**
9	2	$ER = -6.173TL + 1.287Di + 7.489$	9.6994	0.665	26.841**
10	1	$ERP = 5.588Di - 31.087$	41.20552	0.292	11.566**

Sp5 splash erosion for 5% slopes ($\text{g min}^{-1} \text{m}^{-2}$), *Sp40* splash erosion for 40% slopes ($\text{g min}^{-1} \text{m}^{-2}$), *K* soil erodibility factor ($\text{t h MJ}^{-1} \text{mm}^{-1}$), *SE* surface erosion ($\text{t ha}^{-1} \text{year}^{-1}$), *ER* erosion risk ($\text{t ha}^{-1} \text{year}^{-1}$), *ERP* erosion risk potential ($\text{t ha}^{-1} \text{year}^{-1}$), *No* number of trees per hectare (tree), *Di* diameter at breast height of trees (cm), *Ca* canopy cover of trees (%), *He* height of trees (m), *TL* thickness of litter (cm)

**Significant at 0.01 probability level

showed that among the main variables related to vegetation, only the number of trees per hectare and diameter at breast height of trees had significant effect on the splash erosion for 5% slopes. Therefore, the number of trees per hectare and diameter at breast height of trees were selected as the most important variables to estimate splash erosion for 5% slopes in the study area. In addition, among the main variables related to vegetation, only the number of trees per hectare had a significant effect on splash erosion for 40% slopes. Moreover, among the main variables related to vegetation, only the canopy cover and height of trees had significant effects on the soil erodibility factor. Furthermore, among the main variables related to vegetation, only the thickness of surface litter and diameter at breast height of trees had a significant effect on surface erosion and erosion risk. Similarly, Sadeghi et al. (2006) observed strong correlations between canopy cover and surface litter and some erosion parameters in forests. Durán and Rodríguez (2008) also proposed that the canopy cover of plant is the best parameter for estimating the soil loss rate in woodlands and rangelands.

Conclusions

The assessment of soil erosion at 30 burned and unburned sites in the Kanroud forests of northern

Iran showed that the destruction of forest trees by fire had significant effects on erosion rates at the micro-plot and watershed scales. Evaluating erosion at both scales by developing a correlation matrix revealed that there were significant correlations between parameters related to soil erosion at the two scales. This confirmed that the erosion process which may start with splash erosion at the micro-scale finally leads to soil loss at the macro-scale. In addition, it became clear that some vegetation attributes were the most important variables for estimating erosion parameters in the study area. Consequently, the results of this research and new equations developed in this paper may facilitate better soil erosion assessment in the forests of northern Iran. The evaluation of soil loss by mapping the erosion risk at the regional scale is also an important pre-requisite for effective management of the environment and development of policies to address the environmental problems caused by soil erosion. Mapping of the erosion risk potential is also a good way of showing the importance of the cover-management factor in reducing soil loss from forests. Therefore, the protection of forests from fire, monitoring/restricting the activities of forest dwellers and ranchers, preventing the indiscriminate and widespread exploitation of forest resources, and preventing the establishment and development of forest roads will certainly help to reduce the erosion risk in forests.

References

- Abbasian, A. (2012). *Notebook for revised silviculture project in 7 series of Kanroud*. The Company of Tarrahan Alborz Sabz, 342p. (In Persian).
- Aiello, A., Adamo, M., & Canora, F. (2015). Remote sensing and GIS to assess soil erosion with RUSLE3D and USPED at river basin scale in southern Italy. *Catena*, *131*, 174–185.
- Alexakis, D. D., Hadjimitsis, D. G., & Agapiou, A. (2013). Integrated use of remote sensing, GIS and precipitation data for the assessment of soil erosion rate in the catchment area of “Yialias” in Cyprus. *Atmospheric Research*, *131*(1), 108–124.
- Anjos, L. H., Fernandes, M. R., Pereira, M. G., & Franzmeier, D. P. (1998). Landscape and pedogenesis of an oxisol-inseptisols-ultisol sequence in southeastern Brazil. *Soil Science Society of America Journal*, *62*(6), 1651–1658.
- Asadi, H., Vazifedoust, M., Musavi, A., & Honarmand, M. (2011). *Final report on: Assessment and mapping of soil erosion hazard in Navrood watershed (Guilan province) using revised universal soil loss equation (RUSLE), geographic information system (GIS) and remote sensing (RS)*. Guilan Regional Water Company (IWRMC) Deputy of Research and Technical Affairs Applied Research Plan, Islamic Republic of Iran Ministry of Energy. http://www.glrw.ir/uploaded_files/DCMS/wysiwyg/files/research/Final%20Reports/GIR88001.pdf. (In Persian).
- Baharloo, D., Ghorbani Dashtaki, S., Khalil Moghadam, B., Naderi, M., & Tahmasebi, P. (2015). Effects of fire on soil splash erosion in semi-steppe rangeland of Karsanak region, Chaharmahal and Bakhtiari. *Journal of Water and Soil*, *29*(4), 898–907 (In Persian).
- Banj Shafiei, A., Akbarinia, M., Jalali, G., & Alijanpour, A. (2009). Effect of forest fire on diameter growth of beech (*Fagus orientalis* Lipsky) and hornbeam (*Carpinus betulus* L.): a case study in Kheyroud forest. *Iranian Journal of Forest and Poplar Research*, *17*(3), 464–474 (In Persian).
- Bargiel, D., Herrmann, S., & Jadczyzyn, J. (2013). Using high-resolution radar images to determine vegetation cover for soil erosion assessments. *Journal of Environmental Management*, *124*(4), 82–90.
- Battany, M. C., & Grismer, M. E. (2000). Rainfall runoff and erosion in Napa Valley vineyards: effects of slope, cover and surface roughness. *Hydrological Processes*, *14*(7), 1289–1304.
- Bauwer, J. (1986). *Intake rate: cylinder infiltrometer*. In: A. Klute (Ed.), *Methods of soil analysis*. Part 1. 2nd ed. (pp. 341–345). Agron. Monogr. 9. ASA and SSSA, Madison, WI.
- Beguieria, S. (2006). Identifying erosion areas at basin scale using remote sensing data and GIS: a case study in a geologically complex mountain basin in the Spanish Pyrenees. *International Journal of Remote Sensing*, *27*(20), 4585–4598.
- Benavides-Solorio, J., & MacDonald, L. H. (2001). Post-fire runoff and erosion from simulated rainfall on small plots, Colorado Front Range. *Hydrological Processes*, *15*(15), 2931–2952.
- Blake, G. R., & Hartge, K. H. (1986). *Bulk density*. In: A. Klute (Ed.), *Methods of soil analysis*. Part 1. 2nd ed. (pp. 363–375). Agron. Monogr. 9. ASA and SSSA, Madison, WI.
- Brath, A., Montanari, A., & Moretti, G. (2006). Assessing the effect on flood frequency of land use change via hydrological simulation (with uncertainty). *Journal of Hydrology*, *324*(1–4), 141–153.
- Breiman, L., Friedman, J., Olshen, R., & Stone, C. (1984). *Classification and regression trees*. Boca Raton: Chapman & Hall/CRC Press.
- Brevik, E. C., Calzolari, C., Miller, B. A., Pereira, P., Kabala, C., Baumgarten, A., & Jordán, A. (2016). Soil mapping, classification, and pedologic modeling: history and future directions. *Geoderma*, *264*(4), 256–274.
- Chen, T., Niu, R., Li, P., Zhang, L., & Du, B. (2011). Regional soil erosion risk mapping using RUSLE, GIS, and remote sensing: a case study in Miyun Watershed, North China. *Environmental Earth Sciences*, *63*(3), 533–541.
- Conoscenti, C., Di Maggio, C., & Rotigliano, E. (2008). Soil erosion susceptibility assessment and validation using a geostatistical multivariate approach: a test in Southern Sicily. *Natural Hazards*, *46*(3), 287–305.
- Cotler, H., & Ortega-Larrocea, M. P. (2006). Effects of land use on soil erosion in a tropical dry forest ecosystem, Chamela watershed, Mexico. *Catena*, *65*(2), 107–117.
- de Jong, S. M., Brouwer, L. C., & Riezebos, H. T. (1998). *Erosion hazard assessment in the Peyne catchment, France*. Utrecht: Department of Physical Geography, Utrecht University.
- Devall, M. S., Parresol, B. R., & Wright, J. (1995). Dendroecological analysis of *Cordia alliodora*, *Pseudobombax septenatum* and *Annona spraguei* in central Panama. *IAWA Journal*, *16*(4), 411–424.
- Durán, Z. V. H., & Rodríguez, P. C. R. (2008). Soil-erosion and runoff prevention by plant covers. A review. *Agronomy for Sustainable Development*, *28*(1), 65–86.
- Eisazadeh, L., Sokouti, R., Homae, M., & Pazira, E. (2012). Comparison of empirical models to estimate soil erosion and sediment yield in micro catchments. *Eurasian Journal of Soil Science*, *1*(1), 28–33.
- Eisenbies, M. H., Aust, W. M., Burger, J. A., & Adams, M. B. (2007). Forest operations, extreme flooding events, and considerations for hydrologic modeling in the Appalachians—a review. *Forest Ecology and Management*, *242*(2–3), 77–98.
- ESRI (2006). *ArcGIS version 9.2 and the spatial analyst extension*. Redlands: Environmental Systems Research Institute.
- Gee, G. W., & Bauder, J. W. (1986). *Particle size analysis*. In: A. Klute (Ed.), *Methods of soil analysis*. Part 1. 2nd ed. (pp. 383–411). Agron. Monogr. 9. ASA, Madison, WI.
- Ghahraman, B., & Abkhezr, H. (2004). Improvement in intensity-duration-frequency relationships of rainfall in Iran. *Journal of Water and Soil Science*, *8*(2), 1–14 (In Persian).
- Gharemani, A., Ishikawa, Y., Gomi, T., Shiraki, K., & Miyata, S. (2011). Effect of ground cover on splash and sheetwash erosion over a steep forested hillslope: a plot-scale study. *Catena*, *85*(1), 34–47.
- Gorji Bahri, Y., Hematii, A., & Khanjani Shiraz, B. (2012). Effects of tree density on seedling establishment in loblolly pine stand (case study: Pylambra, Guilan). *Iranian Journal of Forest*, *4*(1), 25–32 (In Persian).
- Heydaripour, H. (2013). *Fire in the forests of Guilan province*. Forest, Range and Watershed Organization of Guilan Province, 79p. (In Persian).
- Jafari, A., Finke, P. A., de Wauw, J. V., Ayoubi, S., & Khademi, H. (2012). Spatial prediction of USDA-great soil groups in the

- arid Zaranj region, Iran: comparing logistic regression approaches to predict diagnostic horizons and soil types. *European Journal of Soil Science*, 63(2), 284–298.
- Karaburun, A. (2010). Estimation of C factor for soil erosion modeling using NDVI in Buyukcekmece watershed. *Ozean Journal of Applied Science*, 3(1), 77–85.
- Khalili Moghadam, B., Jabarifar, M., Bagheri, M., & Shahbazi, E. (2015). Effects of land use change on soil splash erosion in the semi-arid region of Iran. *Geoderma*, 241–242, 210–220.
- Kumar, A., Devi, M., & Deshmukh, B. (2014). Integrated remote sensing and geographic information system based RUSLE modelling for estimation of soil loss in western Himalaya, India. *Water Resources Management*, 28(10), 3307–3317.
- Lacoste, M., Lemerrier, B., & Walter, C. (2011). Regional mapping of soil parent material by machine learning based on point data. *Geomorphology*, 133(1–3), 90–99.
- Larsen, I. J., MacDonald, L. H., Brown, E., Rough, D., Welsh, M. J., Pietraszek, J. H., Libohova, Z., & Benavides-Solorio, J. D. D. (2009). Causes of post-fire runoff and erosion: water repellency, cover, or soil sealing? *Soil Science Society of America Journal*, 73(4), 1393–1407.
- LEICA Geosystems, (2003). ERDAS™ field guide. Atlanta, Georgia, USA: LEICA Geosystems GIS and Mapping, LLC, 672 p.
- Lin, C. Y., Lin, W. T., & Chou, W. C. (2002). Soil erosion prediction and sediment yield estimation: the Taiwan experience. *Soil and Tillage Research*, 68(2), 143–152.
- Mahler, P. J. (1979). *Manual of land classification for irrigation*. Soil Institute of Iran. Ministry of Agriculture.
- McBratney, A. B., Mendonça-Santos, M. L., & Minasny, B. (2003). On digital soil mapping. *Geoderma*, 117(1–2), 3–52.
- Mirabdollahi Shamsi, M., Bonyad, A., Bakhshandeh Navrood, B., & Torkaman, J. (2013). Study of age effects on growth of beech trees in Lomir forest. *Iranian Forest Ecology Journal*, 1, 1–15 (In Persian).
- Moffet, C. A., Pierson, F. B., Robichaud, P. R., Spaeth, K. E., & Hardegree, S. P. (2007). Modeling soil erosion on steep sagebrush rangeland before and after prescribed fire. *Catena*, 71(2), 218–228.
- Mohammadi, A., Moayeri, M. H., & Heydari, H. (2012). Determination of the absolute harvesting age of Paulownia even-aged stands in Dr. Bahramnia's Forest Management Project. *Iranian Journal of Forest and Poplar Research*, 20(3), 393–401 (In Persian).
- Moore, I. D., & Wilson, J. P. (1992). Length-slope factors for the revised universal soil loss equation: simplified method of estimation. *Journal of Soil and Water Conservation*, 47(5), 423–428.
- Mosayeb Neghad, I., Rostami Shahraji, T., Kahneh, E., & Porbabaii, H. (2007). Evaluation of native broadleaved forest plantations in east of Guilan province. *Iranian Journal of Forest and Poplar Research*, 15(4), 311–319 (In Persian).
- Mosbahi, M., Benabdalla, S., & Boussema, M. R. (2013). Assessment of soil erosion risk using SWAT model. *Arabian Journal of Geosciences*, 6(10), 4011–4019.
- Mueller, T. G., Cetin, H., Fleming, R. A., Dillon, C. R., Karathanasis, A. D., & Shearer, S. A. (2005). Erosion probability maps: calibrating precision agriculture data with soil surveys using logistic regression. *Journal of Soil and Water Conservation*, 60(6), 462–468.
- Namiranian, M. (2007). *Measurement of trees and forest biometry*. Tehran University Press, 574p. (In Persian).
- National Cartographic Center, (2010). Research Institute of NCC, Tehran, Iran. www.ncc.org.ir.
- Nelson, D. W., & Sommers, L. E. 1996. *Total carbon, organic carbon, and organic matter*. In: D. L. Sparks (Ed.), *Methods of soil analysis*. Part 3. 2nd ed. (pp. 961–1010). Agron. Monogr. 9. ASA and SSSA, Madison, WI.
- Norouzi, M., & Ramezanzpour, H. (2012). Effects of flooding and fire on some of soil properties in Lakan forest in Guilan province. *Journal of Water and Soil Science*, 16(61), 291–300 (In Persian).
- Pierson, F. B., Robichaud, P. R., Moffet, C. A., Spaeth, K. E., Williams, C. J., Hardegree, S. P., & Clark, P. E. (2008). Soil water repellency and infiltration in coarse-textured soils of burned and unburned sagebrush ecosystems. *Catena*, 74(2), 98–108.
- Prasannakumar, V., Shiny, R., Geetha, N., & Vijith, H. (2011). Spatial prediction of soil erosion risk by remote sensing, GIS and RUSLE approach: a case study of Siruvani river watershed in Attapady valley, Kerala, India. *Environmental Earth Sciences*, 64(4), 965–972.
- Providali, I., Elsenbeer, H., & Conedera, M. (2002). Post-fire management and splash erosion in a chestnut coppice in southern Switzerland. *Forest Ecology and Management*, 162(2–3), 219–229.
- Quinlan, J. R. (2001). *Cubist: an informal tutorial*. <http://www.rulequest.com>.
- Quirk, J. P., & Murray, R. S. (1991). Towards a model for soil structure behavior. *Australian Journal of Soil Research*, 29(6), 829–867.
- Rahman, M. R., Shi, Z. H., & Chongfa, C. (2009). Soil erosion hazard evaluation—an integrated use of remote sensing, GIS and statistical approaches with biophysical parameters towards management strategies. *Ecological Modelling*, 220(13–14), 1724–1734.
- Renard, K. G., & Freimund, J. R. (1994). Using monthly precipitation data to estimate the R factor in the revised USLE. *Journal of Hydrology*, 157(1–4), 287–306.
- Renard, K. G., Foster, G. R., Weesies, G. A., & Porter, J. P. (1991). RUSLE—revised universal soil loss equation. *Journal of Soil and Water Conservation*, 46(1), 30–33.
- Renschler, C. S., & Harbor, J. (2002). Soil erosion assessment tools from point to regional scales—the role of geomorphologists in land management research and implementation. *Geomorphology*, 47(2–4), 189–209.
- Rezaie Pasha, M., Kavian, A., & Vahabzade, G. H. (2012). Experimental study of splash erosion and its relation with some soil properties in three adjacent land uses (a case study: Kasilian Watershed). *Journal of Water and Soil Science*, 15(58), 257–269 (In Persian).
- Robichaud, P. R. (2000). Fire effects on infiltration rates after prescribed fire in Northern Rocky Mountain forests, USA. *Journal of Hydrology*, 231–232, 220–229.
- Sadegh, A. (2011). Effect of harvesting on renewal life of *Pinus taeda* and some soil properties (case study: silviculture area of *Pinus taeda* in Pylambra of Guilan province). M.Sc. thesis of silviculture, University of Guilan, 72p. (In Persian).
- Sadeghi, S. H. R. (1995). *Simple visual methods for recognition of sensitive watersheds*. Watershed Management Department, Tarbiat Modarres University, 12p. (In Persian)

- Sadeghi, S. H. R., Safaeian, N. A., & Ghanbari, S. A. (2006). Study on the effect of land uses on type and intensity of soil erosion. *Journal of Agriculture & Engineering Research*, 7(26), 85–98 (In Persian).
- Soil Survey Staff, (2014). *Keys to soil taxonomy*. U.S. Department of Agriculture, Natural Resources Conservation Service.
- SPSS, (1999). *Statistics Package for the Social Sciences*. Version 16. Base Application Guide. SPSS, Chicago, Illinois, USA.
- Stoffel, M., Corona, C., Ballesteros-Cánovas, J. A., & Bodoque, J. M. (2013). Dating and quantification of erosion processes based on exposed roots. *Earth-Science Reviews*, 123, 18–34.
- Taghizadeh-Mehrjardi, R., Sarmadian, F., Minasny, B., Triantafyllis, J., & Omid, M. (2014). Digital mapping of soil classes using decision tree and auxiliary data in the Ardakan region, Iran. *Arid Land Research and Management*, 28(2), 147–168.
- Tang, Q., Xu, Y., Bennett, S. J., & Yang, L. (2015). Assessment of soil erosion using RUSLE and GIS: a case study of the Yangou watershed in the Loess Plateau, China. *Environmental Earth Sciences*, 73(4), 1715–1724.
- USDA (1983). *National soil survey handbook. no. 430*. Washington, DC: US Department of Agriculture.
- Van der Knijff, J., Jones, R., & Montanarella, L. (1999). *Soil erosion risk assessment in Italy*. European Soil Bureau, European Commission.
- Vrieling, A. (2006). Satellite remote sensing for water erosion assessment: a review. *Catena*, 65(1), 2–18.
- Vrieling, A., Steven, M., Sterk, G., & Rodrigues, C. S. (2008). Timing of erosion and satellite data: a multi-resolution approach to soil erosion risk mapping. *International Journal of Applied Earth Observation and Geoinformation*, 10(3), 267–281.
- Wainwright, J., Parsons, A. J., & Abrahams, A. D. (2000). Plot-scale studies of vegetation, overland flow and erosion interactions: case studies from Arizona and New Mexico. *Hydrological Processes*, 14(7), 2921–2943.
- Wang, B., Zheng, F., Römkens, M. J. M., & Darboux, F. (2013). Soil erodibility for water erosion: a perspective and Chinese experiences. *Geomorphology*, 187, 1–10.
- Wischmeier, W. H., & Smith, D. D. (1978). Predicting rainfall erosion losses: a guide to conservation planning. In *Agriculture Handbook No. 537*. Washington: USDA 58.
- World Soil Resources Reports (2014). *World reference base for soil resources*. Rome: Food and Agriculture Organization of the United Nations.
- Xu, L., Xu, X., & Meng, X. (2013). Risk assessment of soil erosion in different rainfall scenarios by RUSLE model coupled with information diffusion model: a case study of Bohai Rim, China. *Catena*, 100(1), 74–82.
- Yusefi, A., Farrokhan Firouzi, A., & Khalili Moghaddam, B. (2014). Evaluation of temporal variation of splash erosion in different slopes and agricultural and forest land uses. *Journal of Water & Soil Resources Conservation*, 3(3), 11–19 (In Persian).
- Zavala, L. M., Granged, A. J. P., Jordán, A., & Bárcenas-Moreno, G. (2010). Effect of burning temperature on water repellency and aggregate stability in forest soils under laboratory conditions. *Geoderma*, 158(374), 366.
- Zhao, W., Fu, B., & Qiu, Y. (2013). An upscaling method for cover-management factor and its application in the loess plateau of China. *International Journal of Environmental Research and Public Health*, 10(10), 4752–4766.
- Zink, J. A. (1989). *Physiography and soils*. Enschede: ITC lecture note SOL.4.1., ITC.
- Zobeiry, M. (2005). *Forest inventory*. Tehran University Press, 401p. (In Persian)
- Zobeiry, M. (2007). *Forest biometry*. Tehran University Press, 405p. (In Persian)